1

A Comprehensive Criterion for Threshold of Motion of Bioclastic Sediments under Steady Unidirectional Flow

Lilei Mao, Jiabo Li, and Yoshimitsu Tajima

Department of Civil Engineering, The University of Tokyo, 7-3-1 Hongo, Bunkyo City, Tokyo, 113-8654, Japan.

Corresponding author: Yoshimitsu Tajima (yoshitaji@coastal.t.u-tokyo.ac.jp)

Key Points:

- We recommend determining threshold criteria for skeletal coral grains as functions of particle density and nominal diameter.

- Distinctions in threshold of motion of bioclastic sediments and quartz sand primarily arise from the influences of grain density and shape.

- A new comprehensive criterion improves the prediction of threshold of bioclastic grain motion under steady unidirectional flow.

Abstract

The threshold of motion of bioclastic sediments is the fundamental aspect for understanding of sediment dynamics in coral reef systems while there are currently few studies on its prediction. We conducted laboratory experiments, and showed that the threshold of motion of coral skeletal grains is more appropriately characterized by the nominal diameter and particle density that is defined as the density of grains with its skeletal void filled by the fluid. Distinctions in threshold of motion of observed coral particles and other bioclastic sediments arise from the influences of grain density and shape, resulting in a notable departure from existing empirical thresholds based on quartz sand. We then propose a new formula for estimating critical shear velocity of bioclastic sediments by introducing a grain shape parameter. The new comprehensive criterion improves the understanding of threshold of motion of bioclastic sediments with highly heterogeneous properties under steady unidirectional flow.

Plain Language Summary

The shorelines of coral reef islands are composed of various biotype sediments, which are derived from shells and marine organisms such as corals. These sediment grains have different size, density and shape characteristics compared with quartz sand. Understanding the threshold condition at which these sediments initiate to move is essential for prediction of transport and topography changes of coral beach. We used a series of data of preceding studies and our newly conducted experiments to investigate appropriate grain proprieties that well characterize the threshold of motion of coral skeletal grains, and found that particle density and nominal diameter are better than solid density and sieve diameter for determination of the threshold. Finally, we proposed a new comprehensive criterion of the threshold of motion of arbitrary particles including bioclastic grains, accounting for the grain shape effect and the settling velocity difference.

1 Introduction

Coral reef islands, also known as coral cays or atolls, have unique landforms of wave-transported coral debris, sand, and organic material on the surface of submerged coral reefs (Masselink et al., 2020), which are typically found in tropical and subtropical regions. Marine carbonate grains that contribute to the composition of coral coasts are primarily derived from the shells and skeletons of marine organisms like corals, mollusks, and foraminifera (East et al., 2018; Masselink et al., 2021), and are accumulated along nearshore areas through complex hydrodynamic processes driven by nearshore currents and wave actions (Bonesso et al., 2022). Climate change and human activities pose a severe threat to the biodiversity of coral reefs, significantly disrupting the process of carbonate grain accumulation and exerting detrimental effects on coastal stability (Quataert et al., 2015; Ferrigno et al., 2016). These bioclastic sediments exhibit heterogenous density, break-down size, and shape characteristics (Chazottes et al., 2008), and understanding the transport characteristics of these sediments is vital for prediction of beach deformation of coral coast.

The prediction of threshold of sediment motion is a fundamental aspect in the study of sediment transport mechanisms. Since the pioneering work of Shields (1936), numerous experiments have been performed to investigate the threshold of motion of both natural and artificial particles on flat beds under virous flow conditions, including steady unidirectional flow and wave-associated orbital oscillatory current flow. Shields curve determines the critical Shields

58 parameter, defined as nondimensional critical shear stress, as a function of a grain Reynolds
59 number. Following the original Shields curve, Paphitis (2001) proposed threshold curves and
60 envelopes to account for the irregular shape of natural particles. Compared to quartz sediments,
61 few studies have investigated the threshold of motion of marine carbonate grains despite their
62 widespread presence in modern and past marine sedimentary environments.

63   Experimental studies on threshold of motion of bioclastic sediments have shown the
64 influence of irregular grain shape on their initiation motion conditions by examining the
65 discrepancy between obtained critical Shields parameter and the existing Shields curve
66 established for quartz sediments (e.g., Rieux et al., 2019; Bian et al., 2023). Some of these
67 preceding studies used alternative grain diameters, e.g., nominal diameter, equivalent settling
68 diameter, to account for the shape effect in formulation of the threshold criteria (e.g., Smith and
69 Cheung, 2004; Weill et al., 2010). Additionally, Movability number, defined as a ratio of shear
70 velocity to settling velocity, was suggested as an alternative parameter for determination of
71 sediment motion threshold (e.g., Beheshti and Ataie-Ashtiani, 2008; Simões, 2014) since it may
72 have a merit in accounting for the influence of settling velocity of sediment grains on their
73 threshold of motion. However, none of them has gained universal recognition as generic
74 threshold criteria of various grains. Further modifications may be required for these preceding
75 criteria to enhance their applicability to bioclastic sediments.

76   In this study, our objective is to quantify the influence of grain density and shape on the
77 determination of threshold criteria for bioclastic sediments and to propose a new comprehensive
78 criterion for estimating critical shear velocity of bioclastic sediments with highly heterogeneous
79 properties by introducing a grain shape parameter. To achieve this objective, we experimentally
80 investigate the threshold of motion of coral particles and compare the obtained critical conditions
81 with those of preceding studies.

2 Materials and Methods

82

2.1 Coral debris samples

83

84   We obtained natural coral debris samples from an aquarium market, which were
85 originally from Okinawa Prefecture, Japan. The source samples were dried and then sieved into
86 five size fractions (Figure S1), including 5.60 mm to 6.70 mm (PS1), 4.75 mm to 5.60 mm (PS2),
87 4.00 mm to 4.75 mm (PS3), 3.35 mm to 4.00 mm (PS4), and 2.00 mm to 3.35 mm (PS5). We
88 measured density of original samples using a 50 ml pycnometer and the average solid density
89 ρ_{solid} was measured to be 2.49±0.23 g/cm^3. However, the density of bioclastic grains is notably
90 affected by their skeletal structures. In this study, we use the particle density ρ_p, defined in
91 Equation 1, for determination of sediment transport characteristics (Cuttler et al., 2017).

$$\rho_p = \rho_{solid}(1 - \varphi) + \rho\varphi \qquad (1)$$

92 Here, φ is the skeletal porosity, and ρ is the fluid density. The average φ of present coral debris
93 sample was measured to be 0.42, resulting in the average ρ_p of 1.87±0.13 g/cm^3 (Mao et al.,
94 2023).

95   The sieve diameter d_{sv} for each size fraction was determined based on a logarithmic
96 distribution of sizes between the adjacent sieves. The commonly used size descriptor for
97 irregularly shaped particles, the nominal diameter d_n, is defined as the diameter of a sphere

98 whose volume is equivalent to that of a non-spherical particle, calculated by $d_n = (d_l d_i d_s)^{1/3}$,
99 where d_l, d_i and d_s represent the diameters in the longest, intermediate, and shortest mutually
100 perpendicular axes, respectively. We built a three-dimensional image acquisition system to
101 measure d_l, d_i, d_s and maximum projected area A_{mp}, of coral particles, and further determined
102 several particle shape parameters, i.e. particle flatness d_s/d_i, elongation d_i/d_l, Corey shape
103 factor S_f $(= d_s/(d_l d_i)^{1/2})$.

104 The settling velocity w_s, of coral particles was determined through settling tube
105 experiments. A detailed description of the particle shape measurement and settling tube
106 experimental method can be found in Mao et al. (2023). We measured the particle shape and
107 settling velocity for over 35 particles in each coral debris sample. These particles covered the
108 largest and the smallest grains in each sample. The average values of obtained particle size,
109 shape parameters and settling velocity were used in subsequent calculations for each sample.

110 2.2 Experimental setup

111 Threshold experiments were performed in the oscillatory flow tunnel (OFT, Figure 1a) at
112 the Coastal Engineering Laboratory of the University of Tokyo, which consists of a loop-shape
113 closed conduit. The OFT is equipped with a 570 cm-long and 23.3 cm-high horizontal test
114 section with a glass sidewall on the observational side and a black wooden background board.
115 The test section has a 430 cm-long, 7.6 cm-wide, and 10 cm-deep pocket filled by sediment to
116 create the movable bed. At both ends of the movable bed section, ramps were respectively placed
117 which smoothly connects the movable bed and the fixed bed of the tunnel floor. Sediment traps
118 made of honeycombs were placed at the end of both sides of the test section. In this experiment,
119 movable bed with thickness of 10 cm was created by the five sets of coral debris samples, and
120 unidirectional flow was generated by the pump. The flow velocity was gradually increased until
121 the coral particles initiate to move.
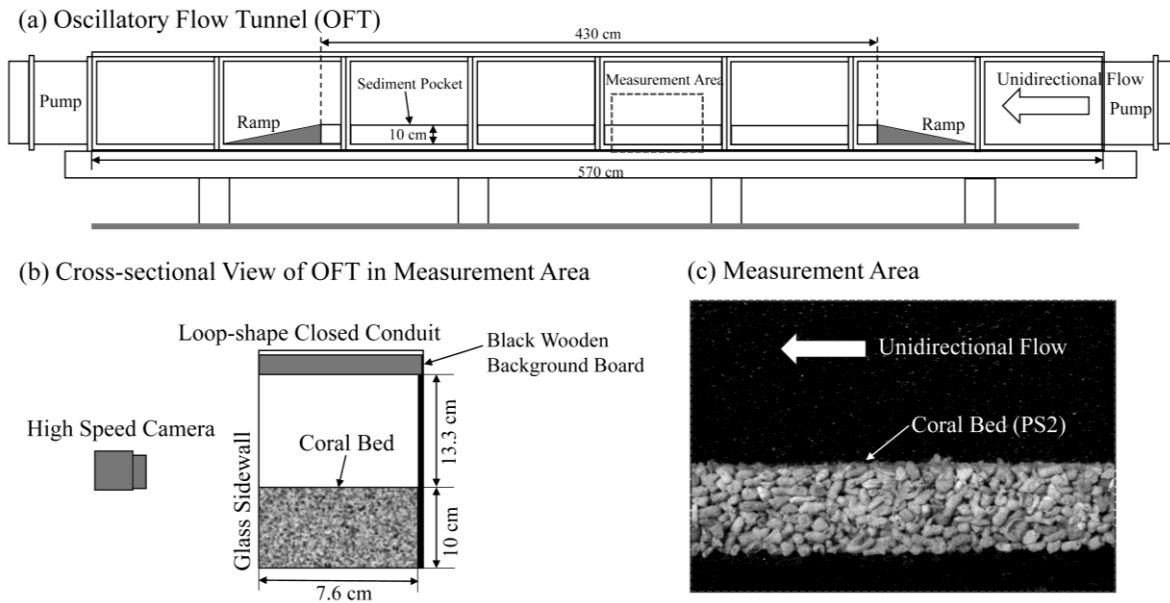

122
123 **Figure 1.** Layout of the threshold experimental setup in the oscillatory flow tunnel.

124 The flow field over the bed was quantified within a rectangular measurement area near
125 the middle part of the test section using a two-dimensional particle image velocimetry (PIV)

126   system. The water was seeded using non-polar crosslinked polymer with a diameter of 0.35 mm
127   and the density nearly identical to the water. Two spotlights were used to illuminate the
128   observation section. The camera was aligned at the average bed level looking normal to the side
129   glass wall (Figure 1b), so that the obtained image accurately captures the streamwise horizontal
130   and vertical flow velocity components. The camera was operated at a frame rate of 120 fps and
131   captured the flow field images with 640×480 pixels in each frame (Figure 1c), which covers the
132   area of 19.4×14.6 cm on the side glass wall.

133   We adopted the quantitative criterion ε (Equation S1) proposed by Yalin (1972) to
134   determine the threshold of motion of coral particles based on the aforementioned video images.
135   The number of grains detached from the bed in a time Δt, over a given area A, of the bed can be
136   estimated by Equation S1, which in turn determines the threshold condition in the experiment. In
137   this study, $\Delta t =120$ sec, $A =0.0266$ m^2, and $\varepsilon \geq 10^{-6}$ were applied to determine the threshold of
138   sediment motion, and the characteristic grain diameter d has been taken as d_n of each sample.

139   A double-averaging method (DAM) (Nikora et al., 2007) was employed to analyze the
140   measured flow field over the coral bed. The bed shear velocity, u_*, can be calculated from the
141   double-averaged (DA) velocity profile within the boundary layer based on the law of the wall
142   (Equation S2). The structure of the boundary layer depends on the hydraulic regime of the flow,
143   which is determined by the shear Reynolds number R_* $(= u_* k_s / \nu$, where k_s is the Nikuradse
144   roughness length and ν is kinetic viscosity of the fluid). The Nikuradse roughness length for
145   hydraulically rough flows is then determined by $k_s = 30z_0$ (Van Rijn, 1993), where z_0 is the
146   level where the DA streamwise horizontal velocity is zero.

147   To compare the threshold of motion of coral particles to other sediment grains, the
148   threshold criteria are represented by critical Shields parameter θ_{cr} and critical Movability
149   number Λ_c, which are respectively defined by,

$$\theta_{cr} = \frac{\rho u_{*cr}^2}{(\rho_s - \rho)gd} \tag{2}$$

$$\Lambda_c = \frac{u_{*cr}}{w_s} \tag{3}$$

150   where ρ_s is the sediment density, and u_{*cr} is the critical shear velocity. Obtained θ_{cr} can be
151   plotted as a function of either the grain Reynolds number Re_* $(= u_* d/\nu)$ or the dimensionless
152   grain diameter d_* $(= [(\rho_s - \rho)g/\rho\nu^2]^{1/3}d)$ (Paphitis, 2001). Experimental parameters at the
153   threshold of motion of the five coral debris samples are reported in Table S1.

3 Results and Discussion

155   3.1 Characterization of particle size, shape, and bed roughness length

156   Figures 2 show characteristics of various grain sizes and shapes of five sets of coral
157   debris samples sorted through sieving. As seen in Figure 2a and Table S1, despite different size
158   ranges, average values of S_f of coral particles in the five samples were close to each other within
159     $0.26 \leq S_f \leq 0.72$, and these S_f values significantly differ from that of the spherical particle
160   ($S_f = 1$). In Figure 2b, the mean intermediate diameter d_i and sieve diameter d_{sv} were linearly
161   correlated, and d_i of all five samples were larger than d_{sv}. Similarly, good linear correlation was
162   found between d_n and d_i (Figure 2c) and between d_n and d_{sv} (Figure 2d) regardless of their

163 particle shapes. The values of d_n were larger than corresponding d_{sv}. These results indicate that
164 the flatness (d_s/d_i) of these sample grains were larger than their elongation (d_i/d_l). This feature
165 also supports the predominance of rod-shaped particles in the five coral debris samples seen in
166 Figure 2a. The obtained linear correlations enable us to reasonably estimate d_i and d_n of coral
167 debris samples as a function of commonly used d_{sv}.

168 Figure 2e shows a clear correlation between S_f and the particle flatness d_s/d_i. Compared
169 to spherical particles, flatter particles have relatively lower effective roughness height, and thus
170 induce lower shear velocities under the same depth-averaged flow velocity. Additionally, we
171 estimated A_{mp} of sample coral particles, which relates to the drag force acting on these particles.
172 Figure 2f shows the plot of observed A_{mp} of coral particles as a function of their d_n. It is evident
173 that A_{mp} of coral particles are larger than that of spherical particle with its diameter represented
174 by d_n, shown in a solid line curve.

175 Relatively large shear Reynolds number, $R_* > 70$, reported in Table S1, indicates that the
176 flow over the coral bed in the experiment is rough-turbulent flow. We obtained the Nikuradse
177 roughness length, k_s, for the five coral beds, and investigated the correlation between estimated
178 k_s and the characteristic grain diameter, d_{sv} or d_n of the coral bed (Figure S2). Good linear
179 correlations were found between k_s and either d_{sv} or d_n for coral beds. It can be reasonably
180 expected that k_s can be determined by any of aforementioned particle diameters since these
181 diameters are also linearly correlated with each other (Figures 2b~2d). The obtained correlations
182 were $k_s \approx 2.68 d_n$ (R^2 =0.99) and $k_s \approx 3.51 d_{sv}$ (R^2 =0.99). The proportionality factor between
183 k_s and d_n was reasonably consistent with Nielsen's (1992) formula ($k_s = 2.5 d_{50}$, where d_{50} is
184 the particle median diameter) for quartz round sand grains. Considering the influence of particle
185 shape difference, we recommend d_n to represent the characteristic size of irregularly shaped
186 coral particles for estimation of k_s and so as threshold criteria. However, further investigation
187 may be required for general merit of d_n since most of existing studies are based on d_{sv} (Weill et
188 al., 2010; Rieux et al., 2019) and the number of studies using d_n is limited.
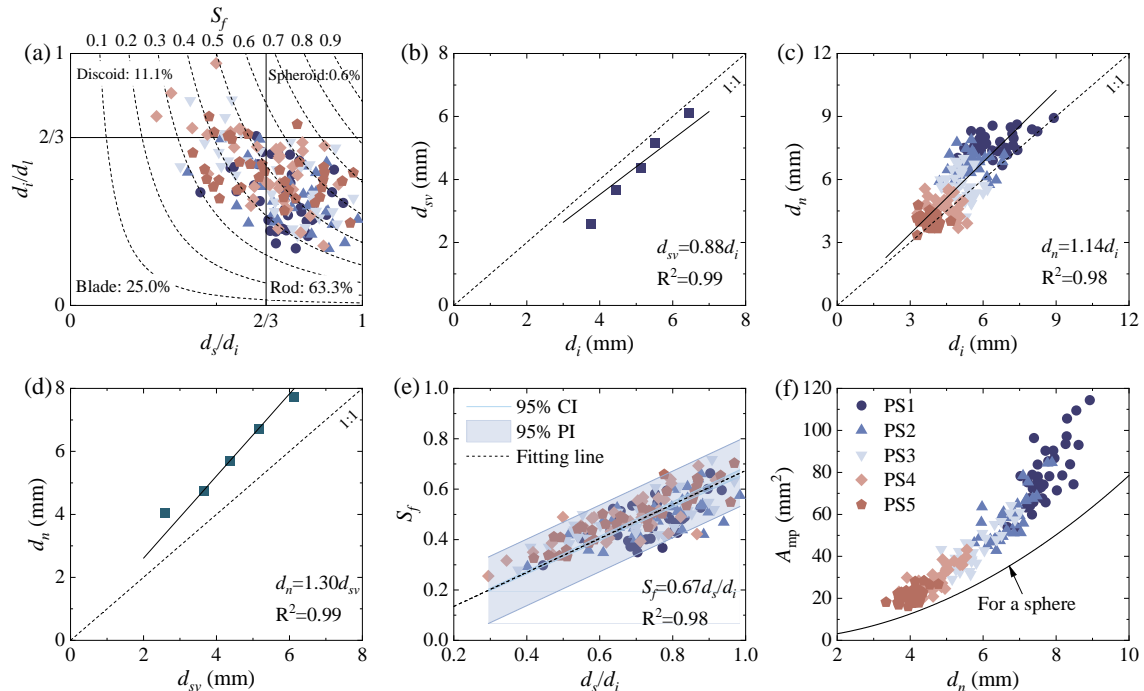

189

Figure 2. Particle size and shape characterization of coral debris samples used in the experiments. (a) Particle shape distribution for each coral debris sample plotted in Zingg classification diagram (1935), where contour lines of the Corey shape factor are shown with their values specified along the top axis. (b) Sieve diameter versus intermediate diameter. (c) Nominal diameter versus intermediate diameter. (d) Nominal diameter versus sieve diameter. (e) Correlation between the Corey shape factor and particle flatness. (f) Relationship between the maximum projected areas A_{mp}, of the particles in the five coral debris samples and their nominal diameters.

3.2 Appropriate grain properties for determination of threshold of bioclastic grain motion

We first calculated critical Shields parameter θ_{cr}, for coral particles using Equation 2 with measured $u_{*\mathrm{cr}}$, $\rho_{\mathrm{s}} = \rho_{\mathrm{p}}$, and $d = d_{sv}$. Figure 3a shows the plot of θ_{cr} for coral particles as a function of d_*. For comparison, this figure shows the plots of θ_{cr} when φ in Equation 1 was set either $\varphi = 0$ and $\varphi = 0.42$. Note that ρ_{p} becomes identical to ρ_{solid} if $\varphi = 0$ is applied. The figure also shows the plots of threshold data of other bioclastic sediments (Table S2 for detailed information) under unidirectional flows (Prager et al., 1996; Paphitis et al., 2002; Smith and Cheung, 2004; Weill et al., 2010; Rieux et al., 2019; Bian et al., 2023). Here $\varphi = 0$ was assumed for these bioclastic grains for determination of ρ_{p} in Figure 3a. While the obtained θ_{cr} based on d_{sv} and ρ_{p} with $\varphi = 0$ for coral particles are close to the empirical curves (Shields, 1936; Paphitis, 2001), the majority of datapoints from preceding studies fall below the empirical curve or even below the lower envelop of Paphitis (2001). For coral particles, values of θ_{cr} increase when the value of φ is changed from 0 to 0.42, and these plots are located even above the upper envelope of Paphitis (2001).

Figure 3b shows the similar plot of θ_{cr} versus d_* for the same particles in Figure 3a but the diameter d in Equation 2 was represented by d_n. An obtained linear relationship $d_n = 1.34 d_{sv}$ (R^2=0.99, Figure S3) was used to estimate d_n of carbonate sand reported by Prager et al. (1996). The d_n values of mollusc fragments (Paphitis et al., 2002; Weill et al., 2010; Rieux et al., 2019) were estimated using $d_n = 0.62 d_{sv}$ (R^2=0.99, Figure S3) based on the shelly particle data of Silva et al. (2023). As seen in the figure, θ_{cr} of coral particles are plotted below the empirical curves (Shields, 1936; Paphitis, 2001) when $\varphi = 0$ is applied. Similarly, datapoints of coral sediment (ρ_{p} =2.82 g/cm^3, $\varphi = 0$) reported by Bian et al. (2023) are also plotted further below the empirical curves (Shields, 1936; Paphitis, 2001) particularly for relatively small d_*. This feature supports our deduction that the grain density neglecting the influence of skeletal porosity, i.e., $\varphi = 0$, is too large to represent the behavior of coral skeletal grains in the fluid. On the other hand, the plot of θ_{cr} versus d_* for coral particles based on ρ_{p} with $\varphi = 0.42$ are slightly above the empirical curves but yet within the 91.1% envelope of Paphitis (2001).

Overall, the use of d_n and ρ_{p} yields θ_{cr} values closer to the empirical curve of Paphitis (2001) (Figure 3b) compared to the use of d_{sv}. From these comparisons, it can be inferred that the combination of d_n and ρ_{p} with appropriate φ would provide a reasonable representation of θ_{cr} for irregular shape coral particles within the range of 4.05 mm< d_n <7.72 mm. While one of drawbacks of d_n and ρ_{p} may be in that it is not easy to obtain their accurate values, accurate estimation of φ may yield θ_{cr} more consistent with the empirical curve. On the other hand, the discrepancy of some datapoints (Figure 3b) may also indicate that empirical Shields curves based on θ_{cr} versus d_* (Shields, 1936; Paphitis, 2001) might not be the best parameter to account for the influence of diverse irregularity of various bioclastic sediments.

The Movability number may have merit in determination of the threshold of bioclastic grain motion because of its explicit inclusion of particle settling velocity. Figures 3c and 3d show the plot of the critical Movability number Λ_c (Equation 3) as a function of d_* based on d_{sv} (3c) and on d_n (3d), respectively, for the present coral particles, other particles and the empirical curve of Simões (2014). In estimation of Λ_c, measured settling velocities were applied except the data reported by Prager et al. (1996), Smith and Cheung (2004) and Bian et al. (2023), in which measured settling velocities were not presented. For these particles, we used the simple formula with their d_n, established for calcareous sand (Equation S3, Alcerreca et al., 2013). The magnitudes of estimated w_s of considered bioclastic grains were smaller than those obtained from the empirical curve based on smooth spheres (Dietrich, 1982).

In Figure 3c, it is evident that the majority of plotted Λ_c are higher than the empirical curve. Many of the plotted Λ_c of mollusc fragments (Rieux et al., 2019) are higher than the empirical curve by a factor of 2 to 3 whereas some of the plotted θ_{cr} of the same mollusc fragments (Rieux et al., 2019) are more than 10 times lower than the Shields curve (Figure 3a). This opposite difference is because the settling velocity of mollusc fragments is much smaller than that of quartz sand grains.

In Figure 3d, some plots are lower than the empirical curve particularly for relatively small d_* based on d_n. Overall better agreement with empirical curve in Λ_c rather than in θ_{cr} indicates the superiority of Λ_c which can account for the influence of various different factors of grains through their settling velocity. Thus, the critical Movability number based on ρ_p and d_n may have the higher potential as a comprehensive criterion for the threshold of motion of bioclastic sediments.
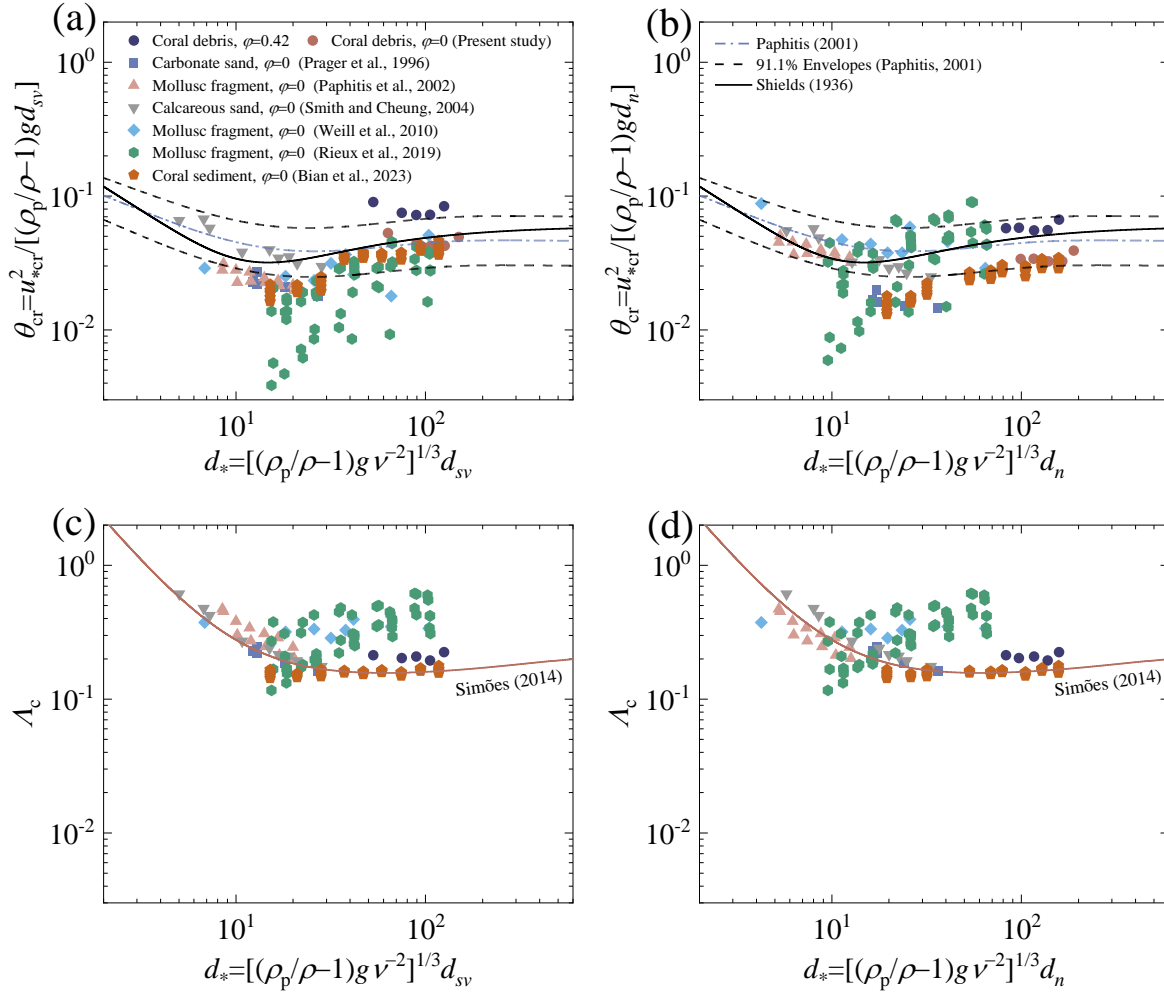
254
255 **Figure 3.** Two threshold criteria, critical Shields parameter θ_{cr} and critical Movability number Λ_c, for coral
256 particles (present study), carbonate sand (Prager et al., 1996), mollusc fragments (Paphitis et al., 2002; Weill et
257 al., 2010; Rieux et al., 2019), calcareous sand (Smith and Cheung, 2004), and coral sediment (Bian et al.,
258 2023). (a) Shields plot (θ_{cr} versus d_*) based on ρ_p and d_{sv}. (b) Shields plot (θ_{cr} versus d_*) based on ρ_p and d_n.
259 (c) Λ_c plot as a function of d_* based on d_{sv}. (d) Λ_c plot as a function of d_* based on d_n. The plotted empirical
260 threshold curves from Shields (1936), Paphitis (2001) and Simões (2014) were developed for the threshold of
261 motion of quartz grains (ρ_s =2.65 g/cm^3) under unidirectional flows.

262   3.3 A new comprehensive criterion for threshold of bioclastic grain motion

263   The determination of Λ_c requires the estimation of w_s of the particle, which depends on
264 the particle density, shape, angularity, and surface roughness (Dietrich, 1982). Similarly, the
265 value of Λ_c may also be affected by these particle characteristics. Accounting for diverse
266 characteristics of particles, we propose a new comprehensive criterion for threshold of motion of
267 bioclastic sediments by,

$$u_{*cr} = w_s \Lambda_c = w_s \Lambda_{c0} f(\text{shape}) \qquad (4)$$

268 where w_s is the settling velocity of the target particle, which accounts for the influence of
269 aforementioned various characteristics of each particle, and Λ_{c0} is the existing empirical formula
270 of the critical Movability number (Simões, 2014) determined by,

$$\Lambda_{c0} = 0.215 + \frac{6.79}{d_*^{1.70}} - 0.075e^{-2.62\times10^{-3}d_*} \tag{5}$$

271   It should be noted that the empirical curve of Simões (2014) is relatively less sensitive to d_*
272   where $d_* > 10$ (Figure 3c), indicating that the choice of d_{sv} or d_n in estimation of Λ_{c0} would
273   yield insignificant difference for relatively large grains of $d_* > 10$. This feature also indicates
274   that the empirical formula (Equation 5) needs further modification to reduce the data dispersion
275   (Figures 3c or 3d) of bioclastic sediments, which may be due to their shape difference. In
276   Equation 4, therefore, $f(\text{shape})$ accounts for the influence of different particle shape on Λ_c
277   while $f(\text{shape}) = 1$ for spherical particles.

278   Taking the logarithm of Equation 4, the following general form is given,

$$\log u_{*cr} = \log \Lambda_{c0} + \log w_s + a\log F \tag{6}$$

279   where a is the fitting coefficient, and F represents a parameter such as S_f, accounting for the
280   shape difference. Following Mao et al. (2023), a ratio of dimensionless settling velocity of an
281   arbitrary particle w_* $(= [(\rho_s - \rho)g\nu/\rho]^{-1/3}w_s)$ to that of a volume-equivalent sphere particle
282   w_{*0}, can also be a candidate option of F, i.e., $F = w_*/w_{*0}$. Estimated w_*/w_{*0} of bioclastic
283   grains in this study are smaller than unity (Figure S4), and thus the shelly particles (Paphitis et al.,
284   2002; Weill et al., 2010; Rieux et al., 2019) are expected to have rather smaller w_*/w_{*0},
285   suggesting a more pronounced influence of $F = w_*/w_{*0}$ on threshold of sediment motion.

286   To achieve the best prediction of u_{*cr}, we conducted regression analysis of Equation 6
287   under different scenarios (Table S3). We assessed the influence of grain shape on prediction of
288   u_{*cr} for present coral grain dataset. When representing F by S_f or, w_*/w_{*0}, Equation 6 yields
289   more accurate prediction of u_{*cr} compared to the scenario with $F = 1$, i.e., $\Lambda_c = \Lambda_{c0}$. Based on
290   the datasets of present coral particles, carbonate sand (Prager et al., 1996), calcareous sand
291   (Smith and Cheung, 2004), and mollusc fragments (Paphitis et al., 2002; Weill et al., 2010;
292   Rieux et al., 2019), we found that $F = w_*/w_{*0}$ yields the best fit formula ($R^2 =0.972$) given by,

$$u_{*cr} = \Lambda_{c0}w_s\left(\frac{w_*}{w_{*0}}\right)^{-0.589} \tag{7}$$

293   Figure 4 shows the comparisons of observed u_{*cr} with predicted u_{*cr} when $F = 1$, i.e.,
294    $\Lambda_c = \Lambda_{c0}$ and the proposed formula (Equation 7). Our proposed formula (Equation 7) yields a
295   lower absolute relative error (ARE) of 14.81%, than the one based on Λ_{c0} with ARE of 35.64%.
296   Either d_{sv} or d_n can be applied for estimation of d_* in Equation (5). As was discussed in the
297   previous section, the choice of either d_{sv} or d_n showed insignificant difference and equally low
298   ARE were obtained in both cases. Considering the limited available information on grain
299   properties, more precise data about skeletal porosity, nominal diameter and shape parameters
300   would further enhance the precision of predicting critical shear velocity using Equation 7 for
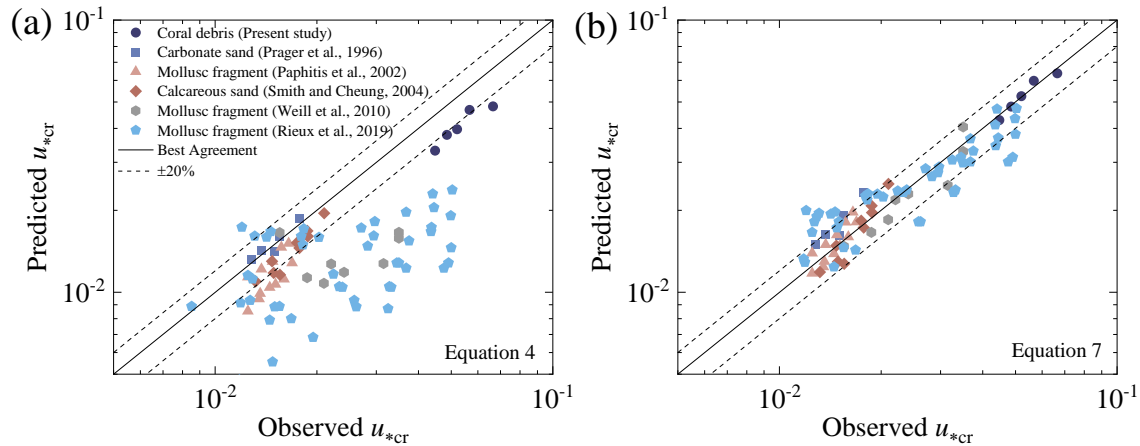301   bioclastic sediments with different size, density and shape.

Figure 4. (a) Comparison of observed u_{*cr} with predicted u_{*cr} when $F = 1$ in Equation 4. (b) Comparison of observed u_{*cr} with predicted u_{*cr} using proposed formula (Equation 7).

4 Conclusions

Our experimental findings from natural coral debris sample, along with compiled data of other bioclastic sediments suggest that the use of particle density and nominal diameter could improve the determination of critical Shields parameter. We quantified the effects of grain density and shape on deriving the threshold criteria for bioclastic sediments versus quartz sand. A new formula for estimating the critical shear velocity of bioclastic sediments was proposed by introducing a grain shape parameter based on the concept of critical Movability number. The new comprehensive criterion improves the predictive skills of threshold of motion of bioclastic sediments under steady unidirectional flow, which may enhance the accurate modeling of sediment dynamics in coral reef systems.

Acknowledgments

Data Availability Statement

Data presented in this paper are available at Zenodo via https://doi.org/10.5281/zenodo.10398426.

References

Alcerreca, J.C., Silva, R., & Mendoza, E. (2013). Simple settling velocity formula for calcareous sand. *Journal of Hydraulic Research*, 51(2), 215-219. doi: 10.1080/00221686.2012.753645

324   Beheshti, A.A., & Ataie-Ashtiani, B. (2008). Analysis of threshold and incipient conditions for

325   sediment movement. *Coastal Engineering*, 55(5), pp.423-430. doi:

326   10.1016/j.coastaleng.2008.01.003

327   Bian, C., Chen, J., Jiang, C., Wu, Z., & Yao, Z. (2023). Threshold of motion of coral sediment

328   under currents in flume experiments. *Sedimentology*. doi: 10.1111/sed.13082

329   Bonesso, J.L., Browne, N.K., Murley, M., Dee, S., Cuttler, M.V., Paumard, V., Benson, D., &

330   O'Leary, M. (2022). Reef to island sediment connections within an inshore turbid reef

331   island system of the eastern Indian Ocean. *Sedimentary Geology*, 436, p.106177. doi:

332   10.1016/j.sedgeo.2022.106177

333   Chazottes, V., Reijmer, J.J.G., & Cordier, E. (2008). Sediment characteristics in reef areas

334   influenced by eutrophication-related alterations of benthic communities and bioerosion

335   processes. *Marine Geology*, 250 (1-2), 114-127. doi: 10.1016/j.margeo.2008.01.002

336   Cuttler, M.V., Lowe, R.J., Falter, J.L., & Buscombe, D. (2017). Estimating the settling velocity

337   of bioclastic sediment using common grain-size analysis techniques. *Sedimentology*, 64(4),

338   987-1004. doi:10.1111/sed.12338

339   Dietrich, W.E. (1982). Settling velocity of natural particles. *Water Resources Research, 18*(6),

340   1615-1626. doi: 10.1029/WR018i006p01615

341   East, H.K., Perry, C.T., Kench, P.S., Liang, Y., & Gulliver, P. (2018). Coral reef island initiation

342   and development under higher than present sea levels. *Geophysical Research Letters*,

343   45(20), pp.11-265. doi: 10.1029/2018GL079589

344   Ferrigno, F., Bianchi, C.N., Lasagna, R., Morri, C., Russo, G.F., & Sandulli, R. (2016). Corals in

345   high diversity reefs resist human impact. *Ecological Indicators*, 70, pp.106-113. doi:

346   10.1016/j.ecolind.2016.05.050

347 Mao, L.L., Li, J.B., Shimozono, T., & Tajima, Y. (2023). Impacts of Particle Shape, Skeletal

348   Porosity and Density on the Settling Velocity of Gravel-Size Coral Debris. *Journal of*

349   *Geophysical Research: Earth Surface*, 128(5), e2022JF006996. doi: 10.1029/2022JF006996

350 Masselink, G., Beetham, E., & Kench, P. (2020). Coral reef islands can accrete vertically in

351   response to sea level rise. *Science Advances*, 6(24), p.eaay3656. doi:

352   10.1126/sciadv.aay3656

353 Masselink, G., McCall, R., Beetham, E., Kench, P., & Storlazzi, C. (2021). Role of future reef

354   growth on morphological response of coral reef islands to sea-level rise. *Journal of*

355   *Geophysical Research: Earth Surface*, 126(2), p.e2020JF005749. doi:

356   10.1029/2020JF005749

357 Nielsen, P. (1992). Coastal Bottom Boundary Layers and Sediment Transport, Advanced Series

358   on Ocean Engineering-Vol. 4. World Scientific: Singapore; 324 pp.

359 Nikora, V., McEwan, I., McLean, S., Coleman, S., Pokrajac, D., & Walters, R. (2007). Double-

360   averaging concept for rough-bed open-channel and overland flows: Theoretical background.

361   *Journal of Hydraulic Engineering*, 133(8), pp.873-883. doi: 10.1061/(ASCE)0733-

362   9429(2007)133:8(873)

363 Paphitis, D. (2001). Sediment movement under unidirectional flows: an assessment of empirical

364   threshold curves. *Coastal Engineering*, 43(3-4), pp.227-245. doi: 10.1016/S0378-

365   3839(01)00015-1

366 Paphitis, D., Collins, M.B., Nash, L.A., & Wallbridge, S. (2002). Settling velocities and

367   entrainment thresholds of biogenic sands (shell fragments) under unidirectional flow.

368   *Sedimentology*, 49(1), pp.211-225. doi: 10.1046/j.1365-3091.2002.00446.x

369   Prager, E.J., Southard, J.B., & VivoniGallart, E.R. (1996). Experiments on the entrainment

370   threshold of well-sorted and poorly sorted carbonate sands. *Sedimentology*, 43(1), pp.33-40.

371   doi: 10.1111/j.1365-3091.1996.tb01457.x

372   Quataert, E., Storlazzi, C., Van Rooijen, A., Cheriton, O., & Van Dongeren, A. (2015). The

373   influence of coral reefs and climate change on wave-driven flooding of tropical coastlines.

374   *Geophysical Research Letters*, 42(15), pp.6407-6415. doi: 10.1002/2015GL064861

375   Rieux, A., Weill, P., Mouaze, D., Poirier, C., Nechenache, F., Perez, L., & Tessier, B. (2019).

376   Threshold of motion and settling velocities of mollusc shell debris: Influence of faunal

377   composition. *Sedimentology*, 66(3), pp.895-916. doi:10.1111/sed.12521

378   Shields, A. (1936). Application of Similarity Principles and Turbulence Research to Bed-load

379   Movement (English Translation of the original German Manuscript). Hydrodynamics

380   Laboratory, California Institute of Technology, Publication No. 167.

381   Silva, F.R.S.D., Borges, A.L.D.O., Toldo Jr, E.E., Fick, C., Puhl, E., Oliveira, V.C.B., & Cruz,

382   F.E.G.D. (2023). Threshold of motion and orientation of bivalve shells under current flow.

383   *Brazilian Journal of Geology*, 53, p.e20220080. doi: 10.1590/2317-4889202320220080

384   Simões, F.J. (2014). Shear velocity criterion for incipient motion of sediment. *Water Science and*

385   *Engineering*, 7(2), pp.183-193. doi: 10.3882/j.issn.1674-2370.2014.02.006

386   Smith, D.A., & Cheung, K.F. (2004). Initiation of motion of calcareous sand. *Journal of*

387   *Hydraulic Engineering*, 130(5), pp.467-472. doi: 10.1061/(ASCE)0733-

388   9429(2004)130:5(467)

389   Van Rijn, L. (1993). Principles of Sediment Transport in Rivers, Estuaries and Coastal Seas.

390   Aqua Publications, Amsterdam, The Netherlands, 690 pp.

391   Weill, P., Mouazé, D., Tessier, B., & Brun-Cottan, J.C. (2010). Hydrodynamic behaviour of

392   coarse bioclastic sand from shelly cheniers. *Earth Surface Processes and Landforms*,

393   35(14), pp.1642-1654. doi: 10.1002/esp.2004

394   Yalin, M.S. (1972). Mechanics of Sediment Transport. Pergamon Press, New York, 290 pp.

395   Zingg, T. (1935). Beitrag zur Schotteranalyse. *Doctoral dissertation, ETH Zurich*. doi:

396   10.3929/ethz-a-000103455

397   **References From the Supporting Information**

398   Padhi, E., Penna, N., Dey, S., & Gaudio, R. (2018). Hydrodynamics of water-worked and

399   screeded gravel beds: A comparative study. *Physics of Fluids*, 30(8). doi:

400   10.1063/1.5044479